Numerical studies of the new color confinement mechansim

Tsuneo Suzuki[1, *]

[1] *Kanazawa University, Kanazawa 920-1192, Japan*

The author proposed recently a new scheme for color confinement based on monopoles in QCD coming from line singularities of non-Abelian gauge fields. To check if the scenario is realized in nature, numerical studies are done extensively in the framework of lattice field theory by adopting pure $SU(2)$ gauge theory as a model of QCD. Monopole dominance of the string tension and the dual Meissner effect caused by monopole currents are found beautifully without any additional gauge fixing. In addition, a blockspin transformation and the Monte-Carlo renormalization group studies are applied to lattice monopoles. With the help of various techniques smoothing the vacuum, it is found that the density of the color-invariant lattice monopole and the effective monopole action show beautiful scaling behaviors. These numerical data suggest that the new confinement scenario is realized in nature. This report shows the highlights of these interesting results obtained mainly by using Large-Scale Computer System of RCNP.

PACS numbers: 11.15.Ha,14.80.Hv,11.10.Wx

I. INTRODUCTION

Color confinement in quantum chromodynamics (QCD) is still an important unsolved problem [1]. As a picture of color confinement, 't Hooft [2] and Mandelstam [3] conjectured that the QCD vacuum is a kind of a magnetic superconducting state caused by condensation of magnetic monopoles and an effect dual to the Meissner effect works to confine color charges. However, to find color magnetic monopoles which condense is not straightforward in QCD.

An interesting idea to realize this conjecture is to project QCD to the Abelian maximal torus group by a partial (but singular) gauge fixing [4]. In $SU(3)$ QCD, the maximal torus group is Abelian $U(1)^2$. Then color magnetic monopoles appear as a topological object. Condensation of the monopoles causes the dual Meissner effect.

Numerically, an Abelian projection in non-local gauges such as the maximally Abelian (MA) gauge has been found to support the Abelian confinement scenario beautifully [5].

However, although numerically interesting, the idea of Abelian projection[4] is theoretically very unsatisfactory. 1) In non-perturabative QCD, any gauge-fixing is not necessary at all. There are infinite ways of such a partial gauge-fixing and whether the 't Hooft scheme is gauge independent or not is not known. 2) After an Abelian projection, only one (in $SU(2)$) or two (in $SU(3)$) gluons are photon-like with respect to the residual $U(1)$ or $U(1)^2$ symmetry and the other gluons are massive charged matter fields. Such an asymmetry among gluons is unnatural. Moreover, also numerically, there are some data suggesting the problem of the 'tHooft idea obtained in a local unitary gauge called Polyakov (PL) gauge [6, 7].

Recently, the present author proposed a new theoretical scheme for color confinement based on the dual Meissner effect which is free from the above problems [8, 9]. The singularities of original gauge fields is found to be the origin of color magnetic monopoles. This is the first in non-Abelian QCD to find Abelian-like monopoles without resorting to any artificial technique. In the next section, we briefly review the above breakthrough in QCD monopole and the new scheme of color confinement.

To prove if such a new confinement scheme is realized in nature, numerical studies in the framework of lattice gauge theories are very important. Section III deals with numerical results showing perfect monopole dominance of the string tension and the Abelian dual meissner effect without any artificial gauge fixing. Section IV discusses the continuum limit of the lattice monopole density and the final section is devoted to the Monte-Carlo renormalization-group studies of the infrared monopole action.

II. A NEW SCHEME OF COLOR CONFINEMENT

A. Equivalence of J_μ and k_μ

First of all, we prove that the Jacobi identities of covariant derivatives lead us to conclusion that violation of the non-Abelian Bianchi identities (VNABI) J_μ is nothing but an Abelian-like monopole k_μ defined by violation of the Abelian-like Bianchi identities without gauge-fixing [8, 9]. Define a covariant derivative operator $D_\mu = \partial_\mu - igA_\mu$. The Jacobi identities are expressed as

$$\epsilon_{\mu\nu\rho\sigma}[D_\nu, [D_\rho, D_\sigma]] = 0. \quad (1)$$

*e-mail:suzuki04@staff.kanazawa-u.ac.jp

By direct calculations, one gets

$$\begin{aligned}[D_\rho, D_\sigma] &= [\partial_\rho - igA_\rho, \partial_\sigma - igA_\sigma] \\ &= -ig(\partial_\rho A_\sigma - \partial_\sigma A_\rho - ig[A_\rho, A_\sigma]) + [\partial_\rho, \partial_\sigma] \\ &= -igG_{\rho\sigma} + [\partial_\rho, \partial_\sigma],\end{aligned}$$

where the second commutator term of the partial derivative operators can not be discarded, since gauge fields may contain a line singularity. Actually, it is the origin of the violation of the non-Abelian Bianchi identities (VNABI) as shown in the following. The non-Abelian Bianchi identities and the Abelian-like Bianchi identities are, respectively: $D_\nu G^*_{\mu\nu} = 0$ and $\partial_\nu f^*_{\mu\nu} = 0$. The relation $[D_\nu, G_{\rho\sigma}] = D_\nu G_{\rho\sigma}$ and the Jacobi identities (1) lead us to

$$\begin{aligned}J_\mu &= \frac{1}{2}J^a_\mu \sigma^a = D_\nu G^*_{\mu\nu} = \frac{1}{2}\epsilon_{\mu\nu\rho\sigma} D_\nu G_{\rho\sigma} \\ &= -\frac{i}{2g}\epsilon_{\mu\nu\rho\sigma}[D_\nu, [\partial_\rho, \partial_\sigma]] = \frac{1}{2}\epsilon_{\mu\nu\rho\sigma}[\partial_\rho, \partial_\sigma]A_\nu \\ &= \partial_\nu f^*_{\mu\nu} = k_\mu = \frac{1}{2}k^a_\mu \sigma^a, \end{aligned} \tag{2}$$

where $f_{\mu\nu}$ is defined as $f_{\mu\nu} = \partial_\mu A_\nu - \partial_\nu A_\mu = (\partial_\mu A^a_\nu - \partial_\nu A^a_\mu)\sigma^a/2$. Namely Eq.(2) shows that the violation of the non-Abelian Bianchi identities is equivalent to that of the Abelian-like Bianchi identities. The Abelian-like monopole satisfies the Abelian-like conservation law

$$\partial_\mu k_\mu = \partial_\mu \partial_\nu f^*_{\mu\nu} = 0 \tag{3}$$

due to the antisymmetric property of the Abelian-like field strength. Hence VNABI satisfies also the same Abelian-like conservation law

$$\partial_\mu J_\mu = 0. \tag{4}$$

B. Dirac quantization condition

Next we show that the magnetic charges derived from $k_4 = J_4$ satisfy the Dirac quantization condition with respect to magnetic and electric charges. Consider a space-time point O where the Bianchi identities are violated and a three-dimensional sphere V of a large radius r from O. Since $k_4 = J_4$ is given by the total derivative, the behavior of the gauge field at the surface of the sphere is relevant. When $r \to \infty$, the non-Abelian field strength should vanish since otherwise the action diverges. Then the magnetic charge could be evaluated by a gauge field described by a pure gauge $A_\mu = \Omega\partial_\mu\Omega^\dagger/ig$, where Ω is a gauge transformation matrix satisfying $\Omega[\partial_\mu, \partial_\nu]\Omega^\dagger = 0$ at $r \to \infty$. Then the magnetic charge g^d_m in a color direction is evaluated as follows:

$$\begin{aligned}g^d_m &= \int_V d^3x k^d_4 = \int d^3x \frac{1}{2}\epsilon_{4\nu\rho\sigma}\partial_\nu(\partial_\rho A^d_\sigma - \partial_\sigma A^d_\rho) \\ &= \int_V d^3x \frac{1}{2ig}\epsilon_{ijk}\partial_i \mathrm{Tr}\sigma^d(\partial_j\Omega\partial_k\Omega^\dagger - \partial_k\Omega\partial_j\Omega^\dagger \\ &\quad +\Omega[\partial_j, \partial_k]\Omega^\dagger) \\ &= \int_V d^3x \frac{1}{2g}\epsilon_{ijk}\{\epsilon^{abc}\partial_i(\hat{\phi}^a\partial_j\hat{\phi}^b\partial_k\hat{\phi}^c \\ &\quad +\partial_i \mathrm{Tr}\sigma^d\Omega[\partial_j, \partial_k]\Omega^\dagger)\} \\ &= \int_{\partial V} d^2S \frac{1}{2g}\epsilon_{ijk}\epsilon^{abc}\hat{\phi}^a\partial_j\hat{\phi}^b\partial_k\hat{\phi}^c, \end{aligned} \tag{5}$$

where $\Omega[\partial_j, \partial_k]\Omega^\dagger = 0$ on the surface at $r \to \infty$ is used and $\hat{\phi}$ is a Higgs-like field defined as

$$\begin{aligned}\hat{\phi} &= \hat{\phi}^i\sigma^i \\ &= \Omega\sigma^d\Omega^\dagger.\end{aligned}$$

$\hat{\phi}^2 = 1$ is shown easily. Since the field $\hat{\phi}$ is a single-valued function, Eq.(5) is given by the wrapping number n characterizing the homotopy class of the mapping between the spheres described by $\hat{\phi}^2 = (\hat{\phi}^1)^2 + (\hat{\phi}^2)^2 + (\hat{\phi}^3)^2 = 1$ and $\partial V = S^2$: $\pi_2(S^2) = Z$. Namely

$$g^d_m g = 4\pi n. \tag{6}$$

This is just the Dirac quantization condition. Note that the minimal color electric charge in any color direction is $g/2$. Hence the kinematical conservation law is also topological.

C. Proposal of the vacuum in the confinement phase

Now we propose a new mechanism of color confinement in which VNABI J_μ play an important role in the vacuum. Since VNABI transforms as an adjoint operator, it can be diagonalized by a unitary matrix $V_d(x)$ as follows:

$$V_d(x)J_\mu(x)V_d^\dagger(x) = \lambda_\mu(x)\frac{\sigma_3}{2},$$

where $\lambda_\mu(x)$ is the eigenvalue of $J_\mu(x)$ and is then color invariant but magnetically charged. Note that $V_d(x)$ does not depend on μ due to the Coleman-Mandula theorem. Then one gets

$$\Phi(x) \equiv V_d^\dagger(x)\sigma_3 V_d(x) \tag{7}$$

$$J_\mu(x) = \frac{1}{2}\lambda_\mu(x)\Phi(x), \tag{8}$$

$$\sum_a (J^a_\mu(x))^2 = \sum_a (k^a_\mu(x))^2 = (\lambda_\mu(x))^2. \tag{9}$$

Namely the color electrically charged part and the magnetically charged part are separated out. From (8) and

(4), one gets

$$\partial_\mu J_\mu(x) = \frac{1}{2}(\partial_\mu\lambda_\mu(x)\Phi(x)+\lambda_\mu(x)\partial_\mu\Phi(x)) = 0. \quad (10)$$

Since $\Phi(x)^2 = 1$,

$$\partial_\mu\lambda_\mu(x) = -\lambda_\mu(x)\Phi(x)\partial_\mu\Phi(x) = 0.$$

Hence the eigenvalue λ_μ itself satisfies the Abelian conservation rule.

Furthermore, when use is made of (5), it is possible to prove that

$$\frac{1}{2}\epsilon_{\mu\nu\rho\sigma}\partial_\nu f'_{\mu\nu}(x) = \lambda_\mu(x)\frac{\sigma_3}{2}, \quad (11)$$

where

$$\begin{aligned} f'_{\mu\nu}(x) &= \partial_\mu A'_\nu(x) - \partial_\nu A'_\mu(x) \\ A'_\mu &= V_d A_\mu V_d^\dagger - \frac{i}{g}\partial_\mu V_d V_d^\dagger, \\ &\equiv \frac{A_\mu^{'a}\sigma^a}{2}. \end{aligned}$$

Namely,

$$\begin{aligned} \frac{1}{2}\epsilon_{\mu\nu\rho\sigma}\partial_\nu f_{\rho\sigma}^{'1,2}(x)(x) &= 0 \\ \frac{1}{2}\epsilon_{\mu\nu\rho\sigma}\partial_\nu f_{\rho\sigma}^{'3}(x)(x) &= \lambda_\mu(x). \end{aligned} \quad (12)$$

The singularity appears only in the diagonal component of the gauge field A'_μ.

If one considers for large r

$$\begin{aligned} A'_\mu &\to \Omega\partial_\mu\Omega^\dagger/ig, \\ \hat{\phi} &= \hat{\phi}^i\sigma^i = \Omega\sigma^3\Omega^\dagger, \end{aligned}$$

one can easily see from (12) and (5) that the magnetic charge from the eigenvalue λ_μ also satisfies the Dirac quantization condition (6).

It is very interesting to see that $f_{\mu\nu}^{'3}(x)$ is actually the gauge invariant 'tHooft tensor[10]:

$$f_{\mu\nu}^{'3}(x) = \mathrm{Tr}\,\Phi(x)G_{\mu\nu}(x) + \frac{i}{2g}\mathrm{Tr}\,\Phi(x)D_\mu\Phi(x)D_\nu\Phi(x),$$

in which the field $\Phi(x)$ (7) plays a role of the scalar Higgs field in Ref.[10]. To be noted is that the field $\Phi(x)$ (7) is determined uniquely by VNABI itself in the gluodynamics without any Higgs field nor any (partial) gauge-fixing. The condensation of the gauge-invariant magnetic currents λ_μ does not give rise to a spontaneous breaking of the color electric symmetry. Condensation of the color invariant magnetic currents λ_μ may be a key mechanism of the physical confining vacuum. This is a new scheme of color confinement we are going to propose.

III. MONOPOLE DOMINANCE AND THE ABELIAN DUAL MEISSNER EFFECT.

A. Definition of lattice monopoles

Since the Dirac quantization condition of the magnetic charge is a key point in studying monopoles as a topological object, we adopt an Abelian-like definition of a monopole following DeGrand-Toussaint [11] as a lattice version of VNABI, First, we explain how to extract the Abelian fields and the color-magnetic monopoles from the thermalized non-Abelian SU(2) link variables,

$$U_\mu(s) = U_\mu^0(s) + i\vec{\sigma}\cdot\vec{U}_\mu(s)\ , \quad (13)$$

where $\vec{\sigma} = (\sigma^1, \sigma^2, \sigma^3)$ is the Pauli matrix. An Abelian link variable in one of the color directions is defined as

$$\theta_\mu^a(s) = \arctan(\frac{U_\mu^a(s)}{U_\mu^0(s)}). \quad (14)$$

Then the Abelian field strength tensors are written as

$$\begin{aligned} \Theta_{\mu\nu}^a(s) &= \theta_\mu^a(s) + \theta_\nu^a(s+\hat{\mu}) - \theta_\mu^a(s+\hat{\nu}) - \theta_\nu^a(s) \\ &= \bar{\Theta}_{\mu\nu}^a(s) + 2\pi n_{\mu\nu}^a(s)\ , \end{aligned} \quad (15)$$

where $\bar{\Theta}_{\mu\nu}^a \in [-\pi, \pi]$ and $n_{\mu\nu}^a(s)$ is an integer corresponding to the number of the Dirac strings piercing the plaquette. The monopole currents are then defined by [11]

$$\begin{aligned} k_\nu^a(s) &= \frac{1}{4\pi}\epsilon_{\mu\nu\rho\sigma}\partial_\mu\bar{\Theta}_{\rho\sigma}^a(s+\hat{\nu}) \\ &= -\frac{1}{2}\epsilon_{\mu\nu\rho\sigma}\partial_\mu n_{\rho\sigma}^a(s+\hat{\nu}) \in \mathbb{Z}\ , \end{aligned} \quad (16)$$

where ∂_μ is regarded as a forward difference.

B. Monopole dominance

We investigate the monopole contribution to the static potential in order to examine the role of monopoles for confinement[12, 13]. The monopole part of the Abelian Polyakov loop operator is extracted as follows:

$$\begin{aligned} P_{\mathrm{A}} &= P_{\mathrm{ph}}\cdot P_{\mathrm{mon}}\ , \\ P_{\mathrm{ph}} &= \exp\{-i\sum_{k=0}^{N_t-1}\sum_{s'} D(s+k\hat{4}-s')\partial'_\nu\bar{\Theta}_{\nu 4}(s')\}\ , \\ P_{\mathrm{mon}} &= \exp\{-2\pi i\sum_{k=0}^{N_t-1}\sum_{s'} D(s+k\hat{4}-s')\partial'_\nu n_{\nu 4}(s')\}\ . \end{aligned} \quad (17)$$

We call P_{ph} the photon and P_{mon} the monopole parts of the Abelian Polyakov loop, respectively. Here the color index is dropped for simplicity.

TABLE I: Simulation parameters for the measurement of the static potential. $N_{\rm RGT}$ is the number of random gauge transformations.

β	$N_s^3 \times N_t$	$a(\beta)$ [fm]	$N_{\rm conf}$	$N_{\rm RGT}$
2.20	$24^3 \times 4$	0.211(7)	6000	1000
2.35	$24^3 \times 6$	0.137(9)	4000	2000
2.35	$36^3 \times 6$	0.137(9)	5000	1000
2.43	$24^3 \times 8$	0.1029(4)	7000	4000

1. *Simulation parameters*

We then compute the static potential from the monopole Polyakov loop correlation function in a finite temperature $T \neq 0$ system in the confinement phase. We set $T = 0.8\ T_c$. In order to examine the scaling behavior of the potential, we simulate the Wilson action on the $24^3 \times (N_t = 4, 6, 8)$ lattices. Simulation parameters are summarized in Table I. The lattice spacing $a(\beta)$ is determined by using the Sommer scale ($r_0 = 0.5$ [fm]) at zero temperature.

2. *Noise reduction by gauge averaging*

Since the signal-to-noise ratio of the correlation functions of $P_{\rm A}$, $P_{\rm ph}$ and $P_{\rm mon}$ are still very small with no gauge fixing, we adopt a new noise reduction method [12]. For a thermalized gauge configuration, we produce many gauge copies applying random gauge transformations. Then we compute the operator for each copy, and take the average over all copies. It should be noted that as long as a gauge-invariant operator is evaluated, such copies are identical, but they are not if a gauge-variant operator is evaluated as in the present case. The results obtained with this method are gauge-averaged, thus, gauge-invariant. In practice, we prepare a few thousand of gauge copies for each independent gauge configuration (see Table I).

3. *Results*

We obtain very good signals for the potentials. We fit these potentials to the function $V_{\rm fit}(R)\sigma R - c/R + \mu$ and extract the string tension and the Coulombic coefficient, which are summarized in Table II.

We observe monopole dominance, i.e., the string tension of the static potential from the monopole Polyakov loop correlation function is identical to that of the non-Abelian static potential. It is remarkable that Abelian dominance and monopole dominance for the string tension show the good scaling behavior with respect to the change of lattice spacing. We do not see the volume dependence of the string tension.

TABLE II: Best fitted values of the string tension σa^2, the Coulombic coefficient c, and the constant μa.

$24^3 \times 4$	σa^2	c	μa	FR(R/a)	$\chi^2/N_{\rm df}$
$V_{\rm NA}$	0.181(8)	0.25(15)	0.54(7)	3.9 - 8.5	1.00
$V_{\rm A}$	0.183(8)	0.20(15)	0.98(7)	3.9 - 8.2	1.00
$V_{\rm mon}$	0.183(6)	0.25(11)	1.31(5)	3.9 - 6.7	0.98
$V_{\rm ph}$	$-2(1) \times 10^{-4}$	0.010(1)	0.48(1)	4.9 - 9.4	1.02
$24^3 \times 6$					
$V_{\rm NA}$	0.072(3)	0.49(6)	0.53(3)	4.0 - 9.0	0.99
$V_{\rm A}$	0.073(4)	0.41(7)	1.09(3)	3.7 - 10.9	1.00
$V_{\rm mon}$	0.073(4)	0.44(10)	1.41(4)	3.9 - 9.3	1.00
$V_{\rm ph}$	$-1.7(3) \times 10^{-4}$	0.0131(1)	0.4717(3)	5.1 - 9.4	0.99
$36^3 \times 6$					
$V_{\rm NA}$	0.072(3)	0.48(9)	0.53(3)	4.6 - 12.1	1.03
$V_{\rm A}$	0.073(2)	0.47(6)	1.10(2)	4.3 - 11.2	1.03
$V_{\rm mon}$	0.073(3)	0.46(7)	1.43(3)	4.0 - 11.8	1.01
$V_{\rm ph}$	$-1.0(1) \times 10^{-4}$	0.0132(1)	0.4770(2)	6.4 - 11.5	1.03
$24^3 \times 8$					
$V_{\rm NA}$	0.0415(9)	0.47(2)	0.46(8)	4.1 - 7.8	0.99
$V_{\rm A}$	0.041(2)	0.47(6)	1.10(3)	4.5 - 8.5	1.00
$V_{\rm mon}$	0.043(3)	0.37(4)	1.39(2)	2.1 - 7.5	0.99
$V_{\rm ph}$	$-6.0(3) \times 10^{-5}$	0.0059(3)	0.46649(6)	7.7 - 11.5	1.02

C. The Abelian dual Meissner effect

1. *Correlation function for the field profile around the q-$\bar{q}$ system*

We investigate the correlation function between a Wilson loop W and a local Abelian operator $\mathcal{O}$ connected by a product of non-Abelian link variables (Schwinger line) L,

$$\langle \mathcal{O}(r) \rangle_W = \frac{\langle \mathrm{Tr}\left[L W(R,T) L^\dagger \sigma^1 \mathcal{O}(r) \right] \rangle}{\langle \mathrm{Tr}\left[W(R,T) \right] \rangle} \,. \tag{18}$$

We use the cylindrical coordinate (r, ϕ, z) to parametrize the q-$\bar{q}$ system, where the z axis corresponds to the q-$\bar{q}$ axis and r to the transverse distance. We are interested in the field profile as a function of r on the mid-plane of the q-$\bar{q}$ system.

2. *Simulation parameters*

In this computation, we employ the improved Iwasaki gauge action with the coupling constants $\beta = 1.10$ and 1.28 on the 32^4 lattice, and $\beta = 1.40$ on the 40^4 lattice in order to investigate the scaling behavior of the correlation functions with less finite lattice cutoff effects. Simulation parameters are listed in Table III. The lattice spacings are determined so as to reproduce the physical string tension $\sqrt{\sigma} = 440$ [MeV]. We use the Wilson loop $W(R = 3, T = 5)$ at $\beta = 1.10$, $W(R = 5, T = 5)$ at $\beta = 1.28$ and $W(R = 7, T = 7)$ at $\beta = 1.40$. Note that the physical

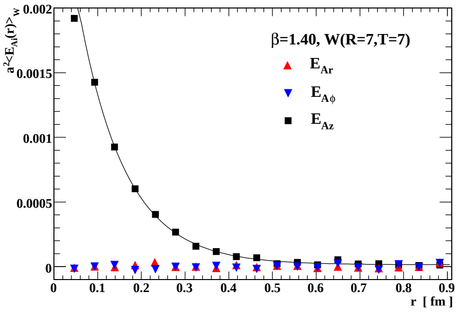

FIG. 1: The profile of the color-electric field $\vec{E}_{\rm A}$ at $\beta = 1.40$.

TABLE III: Simulation parameters for the measurement of the field profile. n and α are the number of smearing steps and the smearing parameter.

β	V	$a(\beta)$ [fm]	$N_{\rm conf}$	n	α
1.10	32^4	0.1069(8)	5000	80	0.2
1.28	32^4	0.0635(5)	6000	80	0.2
1.40	40^4	0.0465(2)	7996	80	0.2

q-$\bar{q}$ distance is the same ($R = 0.32$ [fm]) for these Wilson loops.

3. The penetration depth

We measure all cylindrical components of the color-electric fields $\mathcal{O}(s) = E_{{\rm A}i}(s) = \bar{\Theta}_{4i}(s)$. The results are plotted in Fig. 1. We find that only $E_{{\rm A}z}$ has correlation with the Wilson loop. We then fit $\langle E_{{\rm A}z}(r)\rangle_W$ to a function $f(r) = c_1 \exp(-r/\lambda) + c_0$ and find that the profile of $\langle E_{{\rm A}z}(r)\rangle_W$ is well described by this functional form, i.e., the color-electric field is exponentially squeezed. The fitting curves are also plotted in Fig. 1. The parameter λ corresponds to the penetration depth.

4. The dual Ampère law

To see what squeezes the color-electric field, we study the Abelian (dual) Ampère law derived from the definition of the monopole current in Eq. (16),

$$\vec{\nabla} \times \vec{E}_{\rm A} = \partial_4 \vec{B}_{\rm A} + 2\pi \vec{k}\ , \tag{19}$$

where $B_{{\rm A}i}(s) = (1/2)\epsilon_{ijk}\bar{\Theta}_{jk}(s)$. The correlation of each term with the Wilson loop is evaluated on the same mid-plane of the q-$\bar{q}$ system as for the profile measurements of the color-electric field. We find that only the azimuthal components are non-vanishing, which are plotted in Fig. 2. Note that if the color-electric field is purely of the Coulomb type, the curl of the electric field is zero. On the contrary, the curl of the electric field is non-vanishing and is reproduced mostly by the monopole currents. In any case, the dual Ampère law is satisfied, which is a clear signal of the Abelian dual Meissner effect. This result is quite the same as that observed in the MA gauge [5].

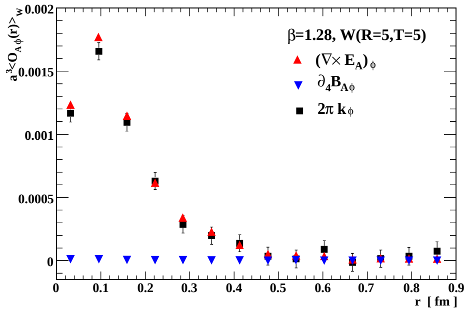

FIG. 2: Tests of the dual Ampère law at $\beta = 1.28$ for $W(R = 5, T = 5)$.

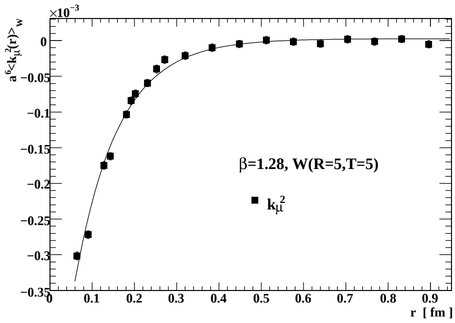

FIG. 3: The profile of the squared monopole currents at 1.28.

5. The coherence length

Let us estimate the coherence length by evaluating the correlation function between the squared monopole density $\mathcal{O}(s) = k_\mu^2(s)$ and the Wilson loop. To measure such a correlation function, we use the disconnected correlation function. We then fit the profile of $\langle k_\mu^2(r)\rangle_W$ to the functional form $g(r) = c_1' \exp(-\sqrt{2}r/\xi) + c_0'$, where the parameter ξ corresponds to the coherence length.

6. The vacuum type

Taking the ratio of the penetration depth and the coherence length, the GL parameter $\sqrt{2}\kappa = \lambda/\xi$ can be estimated, which characterizes the type of the superconducting vacuum. The results are plotted in Fig. **??** against lattice spacing $a(\beta)$. We obtain $\sqrt{2}\kappa = 1.04(7)$, 1.19(5)

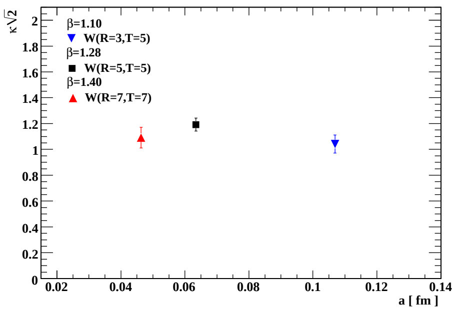

FIG. 4: The GL parameters as a function of the lattice spacing $a(\beta)$.

and 1.09(8) for $\beta = 1.10$, 1.28 and 1.40, respectively.

We find that the GL parameter shows the scaling behavior and the value is about one. This means that the vacuum type is near the border between the type 1 and 2 dual superconductor.

IV. THE CONTINUUM LIMIT OF THE LATTICE MONOPOLE DENSITY.

We adopt the tadpole improved action on 48^4 for coupling constant $\beta = 3.0 \sim 3.9$ and 24^4 for $\beta = 3.3 \sim 3.9$. For other details and other references, see Ref.[9].

A. Smoothing vacuum

1. *Introduction of smooth gauge-fixings*

Monopole loops in the thermalized vacuum produced contain large amount of lattice artifacts. Hence we here adopt a gauge-fixing technique smoothing the vacuum, although any gauge-fixing is not necessary in principle in the continuum limit:

1. Maximal center gauge(MCG).
   We adopt the so-called direct maximal center gauge which requires maximization of the quantity
   $$R = \sum_{s,\mu} (\mathrm{Tr}\, U(s,\mu))^2 \tag{20}$$
   with respect to local gauge transformations. The condition (20) fixes the gauge up to $Z(2)$ gauge transformation.

2. Laplacian center gauge(LCG).
   The second is the direct Laplacian center gauge.

3. Maximal Abelian Wilson loop gauge (AWL).
   The third is the maximal Abelian Wilson loop gauge (AWL) in which
   $$R = \sum_{s,\mu\neq\nu} \sum_{a} (cos(\theta^a_{\mu\nu}(s)) \tag{21}$$
   is maximaized.

TABLE IV: A typical example of monopole loop distributions (Loop length (L) vs Loop number (No.)) for various gauges in one thermalized vacuum on 24^4 lattice at $\beta = 3.6$ in the tadpole improved action. Here I and L denote the color component and the loop length of the monopole loop, respectively.

NGF I=1		MCG I=1		DLCG I=1	
L	No	L	No	L	No
4	154	4	166	4	164
6	20	6	64	6	66
8	7	8	30	8	28
10	2	10	13	10	15
14	1	12	11	12	10
16	1	14	4	14	3
407824	1	16	5	16	6
		18	1	18	2
		22	2	20	1
		24	2	22	1
		28	1	24	2
		30	1	26	3
		32	1	30	1
		34	2	36	1
		36	1	44	1
		44	1	48	1
		46	1	54	1
		48	1	58	1
		58	1	124	1
		124	1	1106	1
		2254	1	1448	1
MAW I=1		MAU1 I=1		MAU1 I=3	
L	No	L	No	L	No
4	142	4	73	4	190
6	66	6	32	6	80
8	36	8	13	8	22
10	8	10	11	10	15
12	7	12	6	12	2
14	3	14	3	14	3
16	3	16	2	16	1
18	1	18	3	18	3
20	1	20	2	20	3
22	3	22	1	24	1
26	3	30	2	36	1
28	1	34	2	42	1
30	2	58	1	60	1
32	1	148	1	66	1
34	1	5188	1	146	1
40	1			318	1
46	1			722	1
58	1				
120	1				
308	1				
1866	1				

TABLE V: The $n = 4$ blocked monopole loop distribution (Loop length (L) vs Loop number (No.)) in various gauges on 6^4 reduced lattice volume at $\beta = 3.6$ in the same vacuum used in TableIV.

NGF I=1		MCG I=1		DLCG I=1	
L	No	L	No	L	No
9266	1	4	5	4	8
		6	1	6	2
		10	1	406	1
		340	1		
AWL I=1		MAU1 I=1		MAU1 I=3	
L	No	L	No	L	No
4	5	4	12	4	8
6	1	6	1	6	3
14	1	10	1	8	2
352	1	24	1	16	1
		26	1	276	1
		270	1		

4. Maximal Abelian and $U(1)$ Landau gauge (MAU1). The fourth is the combination of the maximal Abelian gauge (MAG) and the $U(1)$ Landau gauge. Namely we first perform the maximal Abelian gauge fixing and then with respect to the remaining $U(1)$ symmetry the Landau gauge fixing is done. This case breaks the global $SU(2)$ color symmetry contrary to the previous three cases (MCG, LCG and AWL) but nevertheless we consider this case since the vacuum is smoothed fairly well. MAG is the gauge which maximizes

$$R = \sum_{s,\hat{\mu}} \mathrm{Tr}\Big(\sigma_3 U(s,\mu)\sigma_3 U^{\dagger}(s,\mu)\Big) \tag{22}$$

with respect to local gauge transformations. Then there remains $U(1)$ symmetry to which the Landau gauge fixing is applied, i.e., $\sum_{s,\mu} cos\theta_{\mu}^{3}(s)$ is maximized

2. Extraction of infrared monopole loops

An additional improvement is obtained when we extract important long monopole clusters only from total monopole loop distribution. Let us see a typical example of monopole loop distributions in each gauge in comparison with that without any gauge fixing starting from a thermalized vacuum at $\beta = 3.6$ on 24^4 lattice. They are shown in Table IV. One can find almost all monopole loops are connected and total loop lengths are very large when no gauge fixing is applied as shown in the no gauge-fixing (NGF) case. On the other hand, monopole loop lengths become much shorter in all smooth gauges discussed here. Also it is found that only one or few loops are long enough and others are very short as observed similarly in old papers in MAG. The long monopole clusters are called as infrared monopoles and they are the key ingredient giving confinement. Since small separate monopole loops can be regarded as lattice artifacts, we extract only infrared monopoles alone. We here define as infrared monopoles as all loops having loop lengths longer than 10% of the longest one.

3. Blockspin transformation

Block-spin transformation and the renormalization-group method is known as the powerful tool to study the continuum limit. We introduce the blockspin transformation with respect to Abelian-like monopoles. The idea was first applied in obtaining an infrared effective monopole action in Ref.[14]. The n blocked monopole has a total magnetic charge inside the n^3 cube and is defined on a blocked reduced lattice with the spacing $b = na$, a being the spacing of the original lattice. The respective magnetic currents are defined as

$$\begin{aligned} k_{\mu}^{(n)}(s_n) &= \frac{1}{2}\epsilon_{\mu\nu\rho\sigma}\partial_{\nu} n_{\rho\sigma}^{(n)}(s_n+\hat{\mu}) \\ &= \sum_{i,j,l=0}^{n-1} k_{\mu}(ns_n \\ &\quad +(n-1)\hat{\mu}+i\hat{\nu}+j\hat{\rho}+l\hat{\sigma}), \\ n_{\rho\sigma}^{(n)}(s_n) &= \sum_{i,j=0}^{n-1} n_{\rho\sigma}(ns_n+i\hat{\rho}+j\hat{\sigma}), \end{aligned} \tag{23}$$

where s_n is a site number on the reduced lattice. After the block-spin transformation, the number of short lattice artifact loops decreases while loops having larger magnetic charges appear. We show an example of the loop length and loop number distribution of the four step ($n = 4$) blocked monopoles in TableV with respect to the same original vacuum as in TableIV.

B. Numerical results

Now let us show the simulation results with respect to VNABI (Abelian-like monopole) densities. Since monopoles are three-dimensional objects, the density is defined as follows:

$$\rho = \frac{\sum_{\mu,s_n}\sqrt{\sum_a (k_{\mu}^{a}(s_n))^2}}{4\sqrt{3}V_n b^3}, \tag{24}$$

where $V_n = V/n^4$ is the 4 dimensional volume of the reduced lattice, $b = na(\beta)$ is the spacing of the reduced lattice after n-step blockspin transformation. s_n is the site on the reduced lattice and the superscript a denotes a color component. Note that $\sum_a (k_{\mu}^{a})^2$ is gauge-invariant in the continuum limit. In general, the density ρ is a function of two variables β and n.

1. *Scaling under the block-spin transformations*

It is very interesting to see that more beautiful and clear scaling behaviors are observed when we plot $\rho(a(\beta), n)$ versus $b = na(\beta)$. One can see a universal function $\rho(b)$ for $\beta = 3.0 \sim 3.9$ ($\beta = 3.3 \sim 3.7$) and $n = 1, 2, 3, 4, 6, 8, 12$ ($n = 1, 2, 3, 4, 6$) on 48^4 (24^4) lattice[9]. Namely $\rho(a(\beta), n)$ *is a function of* $b = na(\beta)$ *alone.* Thus we observe clear indication of the continuum ($a(\beta) \to 0$) limit for the lattice VNABI studied in this work.

FIG. 5: Comparison of the VNABI (Abelian-like monopoles) densities versus $b = na(\beta)$ in MCG, AWL, DLCG and MAU1 cases. Here $\rho(b)$ is a scaling function (**??**) determined from the Chi-Square fit to the IF monopole density data in MCG.

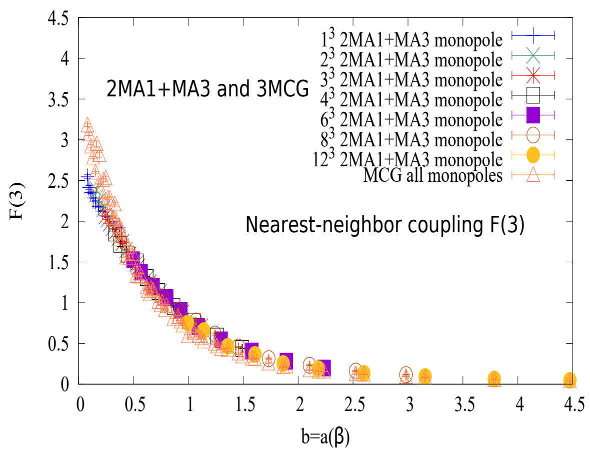

2. *Gauge dependence*

Since $\sum_a (k_\mu^a)^2$ should be gauge-invariant, we compare the data in different smooth gauges. Look at Fig.5, which show the comparison of the data in four gauges (MCG, MAW, DLCG and MAU1). One can see that data obtained in these four different gauges are in good agreement with each other providing strong indication of gauge independence. *This is the main result of this work.* Note that in MAU1 gauge, the global color invariance is broken and usually off-diagonal color components of gauge fields are said to have large lattice artifacts. However here we performed additional U1 Landau gauge-fixing with respect to the remaining $U(1)$ symmetry after MA fixing, which seems to make the vacua smooth enough as those in MCG gauge case. The fact that the scaling functions $\rho(b)$ obtained in MCG gauge can reproduce other three smooth-gauge data seems to show that it is near to the smallest density corresponding to the continuum limit without large lattice artifact effects.

V. INVERSE MONTE-CARLO METHOD AND INFRARED EFFECTIVE MONOPOLE ACTION[15]

A. Inverse Monte-Carlo method

We can determine the infrared monopole action starting from the monopole current ensemble $\{k_\mu^a(s)\}$ with the aid of an inverse Monte-Carlo method. The details of the inverse Monte-Carlo method are reviewed in Appendix of Ref.[15].

Then the monopole action can be written as a linear combination of these operators:

$$\mathcal{S}[k] = \sum_i F(i)\mathcal{S}_i[k], \tag{25}$$

where $F(i)$ are coupling constants. The effective monopole action is defined as follows:

$$e^{-\mathcal{S}[k]} = \int DU(s,\mu)e^{-S(U)} \times \prod_a \delta(k_\mu^a(s) - \frac{1}{2}\epsilon_{\mu\nu\rho\sigma}\partial_\nu n_{\rho\sigma}^a(s+\hat{\mu})),$$

where $S(U)$ is the gauge-field tadpole improved action. We can determine the effective monopole action also starting from the blocked monopole current ensemble $\{K_\mu(s^{(n)})\}$ (23). Then one can obtain the renormalization group flow in the coupling constant space.

Practically, we have to restrict the number of interaction terms. It is natural to assume that monopoles which are far apart do not interact strongly and to consider only short-ranged local interactions of monopoles. The form of actions adopted here are shown in Appendix of [15]. Actually, we study here in details assuming two-point monopole interactions alone, although some four and six point interactions without any color mixing are studied for comparison.

B. Numerical results

The 10 coupling constants $F(i)$ ($i = 1 \sim 10$) of quadratic interactions are fixed very beautifully for lattice coupling constants $3.0 \leq \beta \leq 3.9$ and the steps of blocking $1 \leq n \leq 12$. Remarkablly they are all expressed by a function of $b = na(\beta)$ alone, although they originally depend on two parameters β and n. Namely the scaling is satisfied and the continuum limit is obtained when $n \to \infty$ for fixed $b = na(\beta)$. The obtained action can be considered as the projection of the perfect action onto the plane composed of 10 quadratic coupling constants. The perfect monopole action draws a unique trajectory in the multi-dimensional coupling-constant space. To see if such a behavior is realized in our case, we plot the renormalization group flow line of our data projected onto some two-dimensional coupling-constant planes. These behaviors are shown for the first 3 dominant couplings in Fig.6.

FIG. 6: The renoramlization-group flow projected onto the two-dimensional coupling constant planes in MCG on 48^4.

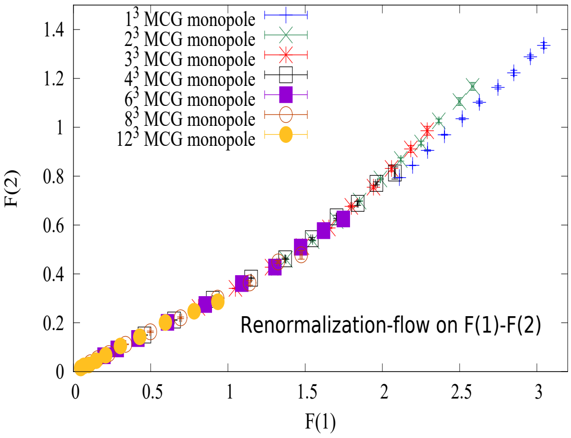

FIG. 7: The coupling constants of the self and the nearest-neighbor interactions in the effective monopole action versus $b = na(\beta)$ in MAU1 and MCG on 48^4. The sum of each coupling constants with respect to three color components are shown.

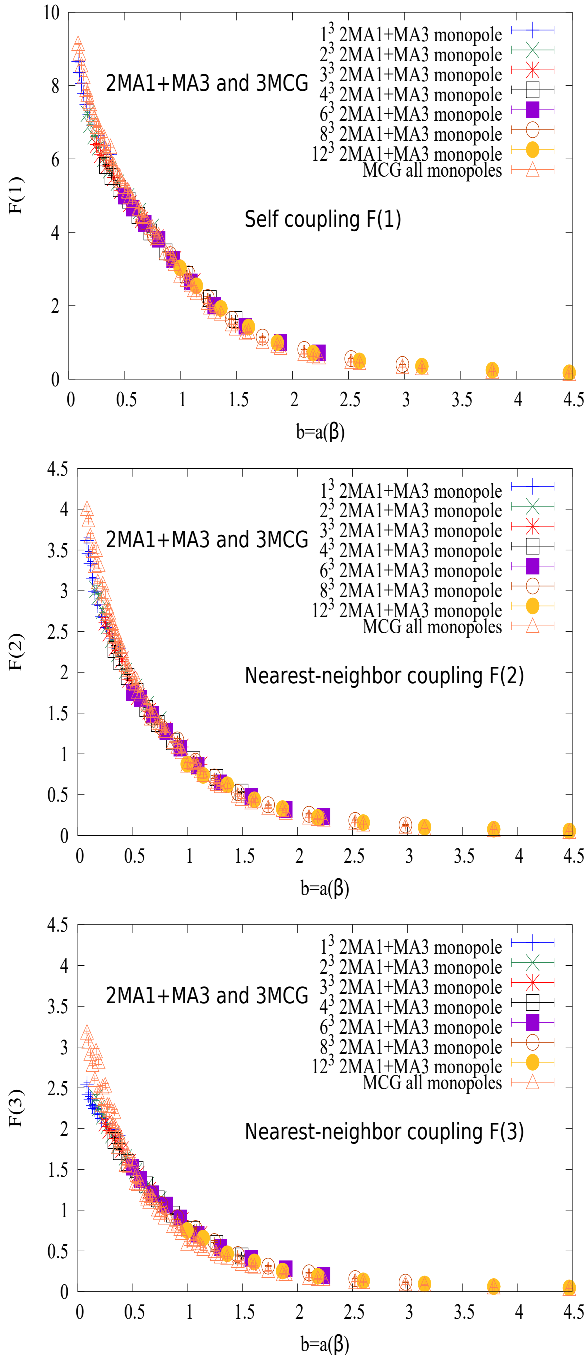

We studied gauge dependence by comparing the data in MCG, DLCG, AWL and MAU1. All data seem to be equal as seen for example from Fig7. This means that if scaling behaviors are obtained and the effective monopole action is on the renormalized trajectory with the introduction of some smooth gauge fixing, the trajectory obtained becomes universal. In fact, the renormalized trajectory represents the effective action in the continuum limit and gauge dependence should not exist in the continuum. It is exciting to see that this natural expectation is realized actually at least for larger b regions $b \geq 0.5$ $(\sigma_{phys}^{-1/2})$.

C. Blocking from the continuum limit

The infrared effective action determined above numerically shows a clear scaling, that is, a function of $b = na(\beta)$ alone and it can be regarded as an action in the continuum limit. But it is an action still formulated on a lattice with the finite lattice spacing $b = na(\beta)$. Hence various symmetries such as rotational invariance of physical quantities in the continuum limit is difficult to observe, since the action itself does not satisfy, say, the rotational invariance. One has to consider a perfect operator in addition to a perfect action on b lattice in order to reproduce a symmetry such as rotational invariance in the continuum limit [16, 17]. It is highly desirable to get a perfect action formulated in the continuum space-time which reproduce the same physics at the scale b as those obtained by the above perfect action formulated on the b lattice. If such a perfect action in the continuum space-time is given, the rotational invariance of physical quantities is naturally reproduced with simple operators such as a simple Wilson loop, since the action also respects the invariance.

If the infrared effective monopole action is quadratic, it is possible to perform analytically the blocking from the continuum and to get the infrared monopole action formulated on a coarse $b = na(\beta)$ lattice [16, 17]. Perfect operators are also obtained.

Let us start from the following action composed of quadratic interactions between magnetic monopole currents. It is formulated on an infinite lattice with very small lattice spacing a:

$$S[k] = \sum_{s,s',\mu} k_\mu(s) D_0(s-s') k_\mu(s'). \tag{26}$$

Here we omit the color index. Since we are starting from the region very near to the continuum limit, it is natural to assume the direction independence of $D_0(s-s')$. Also we adopt only parallel interactions, since we can avoid perpendicular interactions from short-distant terms using the current conservation. Moreover, for simplicity, we adopt only the first three Laurent expansions, i.e., Coulomb, self and nearest-neighbor interactions. Explicitly, $D_0(s-s')$ is expressed as $\bar{\alpha}\delta_{s,s'} + \bar{\beta}\Delta_L^{-1}(s-s') + \bar{\gamma}\Delta_L(s-s')$ where $\bar{\alpha}$, $\bar{\beta}$ and $\bar{\gamma}$ are free parameters. Here $\Delta_L(s-s') = -\sum_\mu \partial_\mu \partial'_\mu \delta_{s,s'}$. Including more complicated quadratic interactions is not difficult.

When we define an operator on the fine a lattice, we can find a perfect operator along the projected flow in the $a \to 0$ limit for fixed b.

Let us start from

$$\begin{aligned}
\langle W_m(\mathcal{C})\rangle &= \sum_{\substack{k_\mu(s)=-\infty \\ \partial'_\mu k_\mu(s)=0}}^{\infty} \exp\{-\sum_{s,s',\mu} k_\mu(s) D_0(s-s') k_\mu(s') \\
&\quad +2\pi i \sum_{s,\mu} N_\mu(s) k_\mu(s)\} \\
&\quad \times \prod_{s^{(n)},\mu} \delta\Big(K_\mu(s^{(n)}) - \mathcal{B}_{k_\mu}(s^{(n)})\Big)/\mathcal{Z}[k], \quad (27)
\end{aligned}$$

where $\mathcal{B}_{k_\mu}(s^{(n)}) \equiv \sum_{i,j,l=0}^{n-1} k_\mu(s(n,i,j,l))$ (23). Note that the monopole contribution to the static potential is given by the term in Eq.(27)

$$\begin{aligned}
W_m(\mathcal{C}) &= \exp\Big(2\pi i \sum_{s,\mu} N_\mu(s) k_\mu(s)\Big), \\
N_\mu(s) &= \sum_{s'} \Delta_L^{-1}(s-s') \frac{1}{2} \epsilon_{\mu\alpha\beta\gamma} \partial_\alpha S^J_{\beta\gamma}(s'+\hat{\mu}), \quad (28)
\end{aligned}$$

where $S^J_{\beta\gamma}(s'+\hat{\mu})$ is a plaquette variable satisfying $\partial'_\beta S^J_{\beta\gamma}(s) = J_\gamma(s)$. Here $J_\mu(s)$ is an Abelian integer-charged electric current corresponding to an Abelian Wilson loop. See Ref. [17].

The cutoff effect of the operator (27) is $O(a)$ by definition. This δ-function renormalization group transformation can be done analytically. Taking the continuum limit $a \to 0$, $n \to \infty$ (with $b = na$ is fixed) finally, we obtain the expectation value of the operator on the coarse lattice with spacing $b = na(\beta)$ [16]:

$$\begin{aligned}
\langle W_m(\mathcal{C})\rangle &= \exp\Bigg\{-\pi^2 \int_{-\infty}^{\infty} d^4x d^4y \sum_\mu N_\mu(x) \\
&\quad \times D_0^{-1}(x-y) N_\mu(y) + \pi^2 b^8 \sum_{\substack{s^{(n)},s^{(n)\prime} \\ \mu,\nu}} B_\mu(bs^{(n)}) \\
&\quad \times D_{\mu\nu}(bs^{(n)} - bs^{(n)\prime}) B_\nu(bs^{(n)\prime})\Bigg\} \\
&\quad \times \sum_{\substack{b^3 K_\mu(bs)=-\infty \\ \partial'_\mu K_\mu=0}}^{\infty} \exp\Bigg\{-S[K_\mu(s^{(n)})] \\
&\quad +2\pi i b^8 \sum_{\substack{s^{(n)},s^{(n)\prime} \\ \mu,\nu}} B_\mu(bs^{(n)}) D_{\mu\nu}(bs^{(n)} - bs^{(n)\prime}) \\
&\quad \times K_\nu(bs^{(n)\prime})\Bigg\} \Bigg/ \sum_{\substack{b^3 K_\mu(bs)=-\infty \\ \partial'_\mu K_\mu=0}}^{\infty} Z[K,0], \quad (29)
\end{aligned}$$

where

$$\begin{aligned}
B_\mu(bs^{(n)}) &\equiv \lim_{\substack{a\to 0 \\ n\to\infty}} a^8 \sum_{s,s',\nu} \Pi_{\neg\mu}(bs^{(n)} - as) \\
&\quad \times \left\{\delta_{\mu\nu} - \frac{\partial_\mu \partial'_\nu}{\sum_\rho \partial_\rho \partial'_\rho}\right\} \\
&\quad \times D_0^{-1}(as - as') N_\nu(as'), \quad (30) \\
\Pi_{\neg\mu}(bs^n - as) &\equiv \frac{1}{n^3} \delta\left(nas^{(n)}_\mu + (n-1)a - as_\mu\right) \\
&\quad \times \prod_{i(\neq\mu)} \left(\sum_{I=0}^{n-1} \delta\left(nas^{(n)}_i + Ia - as_i\right)\right).
\end{aligned}$$

$S[K_\mu(s^{(n)})]$ denotes the effective action defined on the coarse lattice:

$$\begin{aligned}
S[K_\mu(s^{(n)})] &= b^8 \sum_{s^{(n)},s^{(n)\prime}} \sum_{\mu,\nu} K_\mu(bs^{(n)}) \\
&\quad \times D_{\mu\nu}(bs^{(n)} - bs^{(n)\prime}) K_\nu(bs^{(n)\prime}). \quad (31)
\end{aligned}$$

Since we take the continuum limit analytically, the operator (29) does not have no cutoff effect. For clarity, we have recovered the scale factor a and b in (29), (30) and (31).

Performing the BKT transformation explained in Appendix B of Ref. [17] on the coarse lattice, we can get the loop operator for the static potential in the framework of the string model:

$$\begin{aligned}\langle W_m(\mathcal{C})\rangle &= \langle W_m(\mathcal{C})\rangle_{cl} \\ &\times \frac{1}{Z}\sum_{\substack{\sigma_{\mu\nu}(s)=-\infty \\ \partial_{[\alpha}\sigma_{\mu\nu]}(s)=0}}^{\infty} \exp\Big\{-\pi^2 \sum_{\substack{s,s' \\ \mu\neq\alpha \\ \nu\neq\beta}} \sigma_{\mu\alpha}(s)\partial_\alpha\partial'_\beta \\ &\times D^{-1}_{\mu\nu}(s-s_1)\Delta_L^{-2}(s_1-s')\sigma_{\nu\beta}(s') \\ -2\pi^2 &\sum_{\substack{s,s' \\ \mu,\nu}} \sigma_{\mu\nu}(s)\partial_\mu\Delta_L^{-1}(s-s')B_\nu(s')\Big\}, \quad (32)\end{aligned}$$

where $\sigma_{\nu\mu}(s) \equiv \partial_{[\mu}s_{\nu]}$ is the closed string variable satisfying the conservation rule

$$\partial_{[\alpha}\sigma_{\mu\nu]} = \partial_\alpha\sigma_{\mu\nu} + \partial_\mu\sigma_{\nu\alpha} + \partial_\nu\sigma_{\alpha\mu} = 0. \quad (33)$$

The classical part $\langle W_m(\mathcal{C})\rangle_{cl}$ is expressed by

$$\begin{aligned}\langle W_m(\mathcal{C})\rangle_{cl} &= \exp\Big\{-\pi^2\int_{-\infty}^{\infty} d^4x d^4y \sum_\mu N_\mu(x) \\ &\times D_0^{-1}(x-y)N_\mu(y)\Big\}. \quad (34)\end{aligned}$$

FIG. 8: Strong-coupling calculations of the Wilson loops

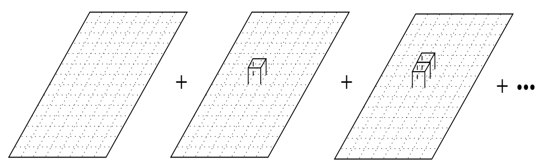

FIG. 9: Comparison of monopole density from MCG numrical data and that from the perfect action

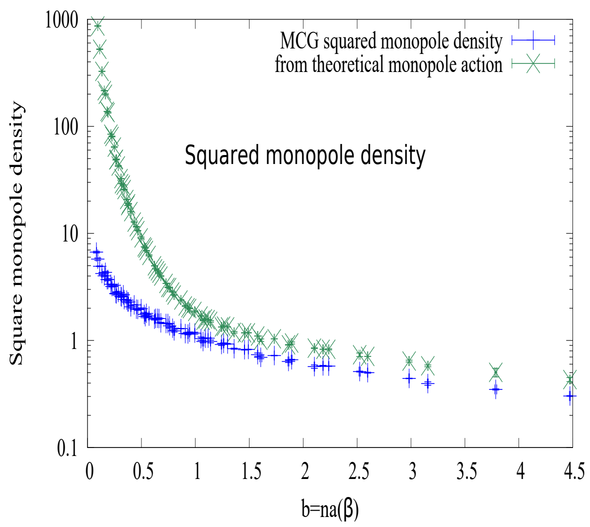

D. Analytic evaluation of non-perturbative quantities

1. Parameter fitting

To derive non-perturbative physical quantites analytically, we have to fix first the propagator $D_0(s)$ in (27) of the continuum limit. It can be done by comparing $D^{-1}_{\mu\nu}(s-s')$ in Eq.(31) with the set of coupling constants $F(i)$ $(i = 1 \sim 10)$ of the monopole action determined numerically in Eq.(25).

$D_0(s-s')$ in the monopole action (27) is assumed to be $\bar{\alpha}\delta_{s,s'} + \bar{\beta}\Delta_L^{-1}(s-s') + \bar{\gamma}\Delta_L(s-s')$. We can consider more general quadratic interactions, but as we see later, this choice is almost sufficient to derive the IR region of SU(2) gluodynamics.

The inverse operator of $D_0(p) = \bar{\alpha} + \bar{\beta}/p^2 + \bar{\gamma}p^2$ takes the form

$$D_0^{-1}(p) = \kappa\left(\frac{m_1^2}{p^2+m_1^2} - \frac{m_2^2}{p^2+m_2^2}\right), \quad (35)$$

where the new parameters κ, m_1 and m_2 satisfy $\kappa(m_1^2 - m_2^2) = \bar{\gamma}^{-1}, m_1^2+m_2^2 = \bar{\alpha}/\bar{\gamma}, m_1^2 m_2^2 = \bar{\beta}/\bar{\gamma}$.

Using Eq.(35) and performing the First Fourier transform(FFT) on a momentum lattice for the several input values κ, m_1 and m_2 we calculate the momentum representation of the blocked monopole action $D_{\mu\nu}(p)$.

To be noted, the three parameters as a function of $b = na(\beta)$ can not be uniquely determined. Moreover m_2/b is found to correpond to the mass of the lowest scalar glueball. Hence we assume

- $m_1/m_2 = 10$ for all $b = na(\beta)$ regions.
- $m_2/b \sim 1.8$ correponding to $M_{0^{++}} \sim 3.7\sqrt{\sigma_{phys}}$.
- The string tension calculated analytically is as near as possible to the physical string tension σ_{phys} and shows scaling, namely σ/σ_{phys} is constant for all $b = na(\beta)$ regions considered.

Table VI shows the results of the best fit. With the parameters determined, the first 5 two-point interactions are fairly well reproduced for large $b > 1.0$ regions.

2. The string tension

Let us evaluate the string tension using the perfect operator (32) [16]. The plaquette variable $S^J_{\alpha\beta}$ in Eq.(28) for the static potential $V(Ib, 0, 0)$ is expressed by

$$\begin{aligned}S^J_{\alpha\beta}(z) &= \delta_{\alpha 1}\delta_{\beta 4}\delta(z_2)\delta(z_3)\theta(z_1) \\ &\times \theta(Ib-z_1)\theta(z_4)\theta(Tb-z_4). \quad (36)\end{aligned}$$

We have seen that the monopole action on the dual lattice is in the weak coupling region for large b. Then the string model on the original lattice is in the strong

TABLE VI: Best parameters fitted

$b = na(\beta)$	0.5	1	1.5	2	2.5	3	3.5	4	4.5
κ	0.117504	0.470017	1.057538	1.880067	2.937605	4.230151	5.757705	7.520268	9.51784
m_1	9	18	27	36	45	54	63	72	81
m_2	0.9	1.8	2.7	3.6	4.5	5.4	6.3	7.2	8.1
$\bar{\alpha}$	8.682261	2.170565	0.964696	0.542641	0.34729	0.241174	0.177189	0.13566	0.107188
$\bar{\beta}$	6.963001	6.963001	6.963001	6.963001	6.963001	6.963001	6.963001	6.963001	6.963001
$\bar{\gamma}$	1.06e-01	6.63e-03	1.31e-03	4.15e-04	1.70e-04	8.19e-05	4.42e-05	2.59e-05	1.62e-05

coupling region. Therefore, we evaluate Eq.(32) by the strong coupling expansion. The method can be shown diagrammatically in Figure 7.

As explicitly evaluated in Ref. [16], the dominant classical part of the string tension coming from Eq. (34) is

$$\sigma_{cl} = \frac{\pi\kappa}{2b^2}\ln\frac{m_1}{m_2}. \tag{37}$$

This is consistent with the analytical results in Type-2 superconductor. The two constants m_1 and m_2 may be regarded as the coherence and the penetration lengths.

The ratio $\sqrt{\sigma_{cl}/\sigma_{phys}}$ using the optimal values κ, m_1 and m_2 given in Table VI becomes a bit higher, namely about 1.3 for all b regions considered. As shown previously [16], quantum fluctuations are so small to recover the difference. This is due mainly to that the assumption of 10 quadratic monopole couplings alone is too simple.

Note that the rotational invariance of the static potential is maintained by the calculation using the classical part as naturally expected from the perfect action. For example, the static potential $V(Ib, Ib, 0)$ can be written as

$$V(Ib, Ib, 0) = \frac{\sqrt{2}\pi\kappa Ib}{2}\ln\frac{m_1}{m_2}. \tag{38}$$

The potentials from the classical part take only the linear form and the rotational invariance is recovered completely even for the nearest $I = 1$ sites.

3. *The lowest scalar glueball mass*

We consider here the following U(1) singlet and Weyl invariant operator

$$\Psi(t) = L^{-3/2}\sum_{\vec{x}} Re\,(\Psi_{12} + \Psi_{23} + \Psi_{31})\,(\vec{x}, t) \tag{39}$$

on the a-lattice at timeslice t. Here $\Psi_{ij}(\vec{x}, t)$ is an $na \times na$ abelian Wilson loop and L stands for the linear size of the lattice. One can check easily that this operator carries 0^{++} quantum number. Then we evaluate the connected two point correlation function of Ψ by using the string model just as done in the case of the calculations of the string tension. It turns out that the quantum correction is also negligibly small for large b. Refer to the paper [17] for details. Assuming the lowest mass gap obtained by the Ψ operator (39) for finite b is the scalar glueball mass, we get the lowest scalar glueball mass as $M_{0^{++}} = 2m_2$. In the best-fit parameters listed in Table VI, we have fixed m_2 so to reproduce $M_{0^{++}}/\sigma_{phys} \sim 3.7$ which is consistent with the direct calculations done in Ref. [18].

4. *Monopole density distribution*

As shown in our previous work [9], the monopole density

$$r(b) \equiv \frac{\rho}{b^3} = \frac{1}{4\sqrt{3}Vb^3}\sum_{s,\mu}\sqrt{\sum_a (K^a_\mu(s))^2} \tag{40}$$

shows beautiful scaling behaviors in smooth gauges such as MCG, where V is the lattice volume. Namely the monopole density (40) can be written in terms of a unique function $r(b)$ of $b = na(\beta)$.

Now we have derived the infrared effective monopole action showing also beautiful scaling. It is interesting to evaluate the monopole density from the effective action analytically. Since the square-root operator is rather difficult to evaluate analytically, we consider the squared monopole density defined as

$$R(b) \equiv \frac{1}{4Vb^3}\sum_{s,\mu}(\sum_a (K^a_\mu(s))^2) \tag{41}$$

The squared density $R(b)$ is plotted in Fig.9 in comparison with that calculated numerically with the help of the MCG data obtained in Ref. [9]. One can see a rough agreement for $b = na(\beta) > 1.2$ ($\sigma_{phys}^{-1/2}$). The difference may comes again from the simple assumption of 10 quadratic interactions alone adopted here. Anyway, the features are new found in the global color-invariant smooth gauge like in MCG.

Acknowledgments

All numerical simulations reported here were done using Large-Scale Computer System at RCNP of Osaka University. The author would like to thank RCNP strongly for their continuous support of computer facilities. He acknowledges also Dr.Katsuya Ishiguro for illuminating discussions and collaborations.

[1] K. Devlin, *The millennium problems : the seven greatest unsolved mathematical puzzles of our time*,Basic Books, New York (2002).
[2] G. 't Hooft, in *Proceedings of the EPS International*, edited by A. Zichichi, p. 1225, 1976.
[3] S. Mandelstam, Phys. Rept. **23**, 245 (1976).
[4] G. 't Hooft, Nucl. Phys. **B190**, 455 (1981).
[5] Y. Koma, M. Koma, E.-M. Ilgenfritz, and T. Suzuki, Phys. Rev. **D68**, 114504 (2003),
[6] M. Chernodub, Phys. Rev. **D69**, 094504 (2004).
[7] T. Sekido, K. Ishiguro, Y. Koma, Y. Mori, and T. Suzuki, Phys. Rev. **D76**, 031501 (2007).
[8] T. Suzuki, A new scheme for color confinement due to violation of the non-Abelian Bianchi identities, arXiv:1402.1294.
[9] T. Suzuki, K. Ishiguro and V. Bornyakov, Phys. Rev. **D97**, 034501 (2018) .
[10] G. 't Hooft, Nucl. Phys. **B79**, 276 (1974).
[11] T. A. DeGrand and D. Toussaint, Phys. Rev. **D22**, 2478 (1980).
[12] T. Suzuki, K. Ishiguro, Y. Koma and T. Sekido, Phys. Rev. **D77**, 034502 (2008).
[13] T. Suzuki, M. Hasegawa, K. Ishiguro, Y. Koma and T. Sekido, Phys. Rev. **D80**, 054504 (2009).
[14] H. Shiba and T. Suzuki, Phys. Lett. **B351**, 519 (1995).
[15] T. Suzuki, arXiv:1712.06812 (2017) (To appear in PRD).
[16] S. Fujimoto, S. Kato and T. Suzuki, Phys. Lett. **B476**, 437 (2000).
[17] M.N.Chernodub et al., Phys. Rev. **D62** 094506 (2000) and references therein.
[18] Biagio Lucini, Michael Teper and Urs Wenger, JHEP **0406**, 012 (2004).